Studies of seismic velocities in subduction zones from continuous OBS data

Weiwei Wang[1], Martha Savage[1], Alec Yates[1], Shu-Huei Hung[2], Yinhe Luo[3], Tim Stern[1], Pei-Ying Patty Lin[4], Hsin-Ying Yang[5], Ban-Yuan Kuo[6], Bill Fry[7], Spahr Webb[8]

[1] School of Geography, Environment and Earth Sciences, Victoria University of Wellington, New Zealand
[2] Department of Geosciences, National Taiwan University, Taiwan
[3] Institute of Geophysics & Geomatics, China University of Geosciences (Wuhan), China
[4] Department of Earth Sciences, National Taiwan Normal University, Taiwan
[5] School of Earth and Space Sciences, University of Science and Technology of China, China
[6] Institute of Earth Sciences, Academia Sinica, Taiwan
[7] GNS Science, New Zealand
[8] Lamont-Doherty Earth Observatory, Columbia University, US

Email address of presenting author: weiwei.wang@vuw.ac.nz

Abstract

In recent years, Ocean Bottom Seismometers (OBSs) have become widely used to expand the coverage of seismic networks onto the ocean. This study takes advantage of offshore observations at the northern end of the Hikurangi margin, New Zealand and southwestern Okinawa Trough to study the tectonics in both regions.

In the Hikurangi subduction zone, slow slip events (SSEs) have been observed, which are caused by the subduction of the Pacific Plate under New Zealand. The behaviour of SSEs and how they influence the physical properties of Earth materials are open to question. From 2014 to 2015, 15 OBSs were deployed offshore Gisborne, New Zealand on the Hikurangi margin. Ambient noise data from the OBSs are used to study velocity changes related to SSEs. Single station cross-component correlations are computed, from which coda waves are used to monitor the velocity changes before, during and after the SSEs in 2014 and 2015 to analyse the slow earthquake behaviour and its relation to stress changes. The horizontal components are rotated to be parallel and perpendicular to the coastline. The dv/v averaged from all the used stations displays a 0.1% velocity decrease at the beginning of the SSE in October 2014, followed by a 0.14% velocity increase.

The southwestern Okinawa Trough is extending and rifting. This study is to determine a shear wave velocity structure and suggest its relation to the back-arc rifting. At various times between 2010 and 2017, 22 OBSs on a small scale (~0.2°×0.3°) were deployed in Southwestern Okinawa Trough offshore northeast Taiwan. Ambient noise recorded on vertical velocity and pressure sensors is used to retrieve Scholte waves for studying the shear wave velocity structure. Phase velocities are forward-modeled according to a model proposed by Kuo et al. 2015, shear strength, and density information from ODP1202. Phase velocity dispersion curves are measured from cross-correlations and unwrapped according to which branch of the modeled phase velocities they appear closest to. The results suggest that the velocity in the north of the rifting axis is higher than the velocity in the south. A 3D shear wave velocity inversion will be conducted for a better imaging in the study region.

1. The Hikurangi

1.1 Background and data

Slow slip events (SSE) have been a hot topic as they extend our understanding of subduction behaviours, but they are difficult to observe due to the depth at which most occur. Northern Hikurangi has the advantage to have documented SSE events at relatively shallow depth as well as onshore and offshore seismic sensors to collect crucial data. The behaviour of SSEs and how they influence (or are influenced by) the physical properties of surrounding materials are still open to question. Monitoring velocity changes before, during and after SSEs provides opportunities to study the slow earthquake behaviour and its relation to stress changes.

From May of 2014 to June of 2015, for the project "The Hikurangi Ocean Bottom Investigation into Tremor and Slow Slip (HOBITSS)", 10 OBSs from Lamont Doherty Earth Observatory (LOBS), 5 OBSs from Earthquake Research Institute, Japan (EOBS), were deployed offshore Gisborne (Figure 1-1). We compute the single station cross component correlation functions from continuous data recorded by three component seismometers of 12 OBSs and we use the coda waves to monitor velocity changes.

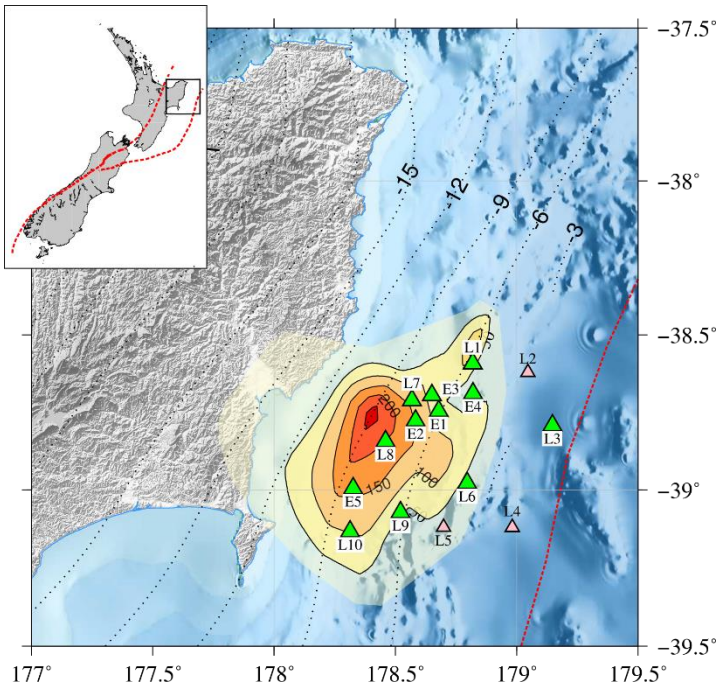

Figure 1-1. Locations of OBSs with a background of slip from a SSE occurring from September to October 2014 (Wallace et al., 2016). Station names are shorten from LOBS to L and EOBS to E. The green triangles denote the stations used in this study and the pink stations are not used because of data quality. Dashed red lines show plate boundary interface (Coffin et al., 1998), and dotted contours show plate interface depth in km (Williams et al., 2013).

1.2 Method

Velocity changes are determined by measuring the time differences between successive current stacks and the reference stack (Brenguier et al., 2008). The reference stack represents a background state of the study region that is stacked by much more days than the current stack, e.g., a reference stack is stacked by all available cross-correlations during the deployment, while the current stack is over 10 days, 20 days, or 30 days.

Figure 1-2 provides an idea on how dv/v can be observed. Scattered waves travel between different channels of a station. Assuming a velocity change under the station happens at some time, reference stack and current stack are computed and compared, and the travel time changes between the reference and current stack can be measured. Velocity change is then determined by dv/v = -dt/t (Lecocq et al., 2014). Usually coda waves are used to measure the delay time because they travel longer, and therefore the delay time is more obvious on coda than the direct arrivals. The delay time computation is carried out by the moving-window cross spectrum analysis (MWCS) (Clarke et al., 2011) moving in scattered wave window of the stacks.

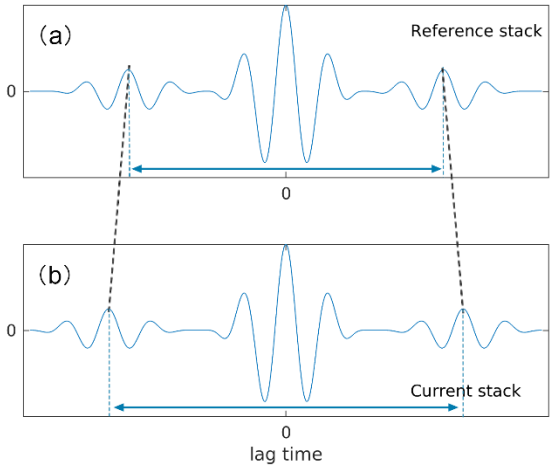

Figure 1-2. Velocity changes measurement sketch. (a) Reference stack. The wave at 0 lag time is the direct arrival and the coda waves at both positive and negative lags are scattered waves. The arrow below them indicates the arrival time of scattered waves. (b) current stack of the same station after the velocity variation.

Seismic noise data are processed through to velocity changes using the Python package MSNoise (Lecocq et al., 2014). Parameterization follows the approach of Yates (2018). Parameters in MSNoise are tested and evaluated by lag-time dependent signal-noise ratio (SNR) (Larose et al. (2007)), coherence and correlation coefficient between current stack and reference stack. Individual and average evaluation values from different stations and components are computed, based on different parameters. The evaluation values with different parameters are compared and the parameters with higher values are chosen.

The following are the main parameters required to be determined. Figure 1-3, Figure 1-4 and Figure 1-5 show some examples of evaluation and comparison of different parameters.

- Filter: different filter ranges are tested and compared by lag-time dependent SNR (Figure 1-3). The values around 0 lag time are not considered because they are for first arrivals. Filters 2.5-6 s and 2.5-20 s have good SNR on coda waves.
- Parameters of segmentation (raw data window length to correlate), segmentation overlap (amount of overlap between data windows), and normalization (1-bit, or windsorizing at N time RMS) are evaluated by lag-time dependent SNR, similar to filter. (not shown)
- Coda wave window: window to compute moving-window cross spectrum analysis (MWCS) is determined by lag-time dependent SNR and coherence (Figure 1-4(a)).
- Threshold of coherence: determined together with SNR (Figure 1-4 (b)).
- MWCS window length: having a larger MWCS window is better for resolving the true velocity change (Yates, 2018) but it cannot be too long within the coda wave widow length.
- MWCS window step: a smaller window step results in higher resolution of dt calculation but costs more time to compute.

- max dt/t: maximum dt is set to 0.5% max lag time. It is set to be 0.2 s when 0.5% max lag time is less than 0.2 s. Setting this threshold is to exclude values that are too large, caused by noise.
- max dt/t error: Errors of computing dt/t are computed and a threshold of 0.1 is set.
- Current stack: Correlation coefficients between different size current stacks and reference stack are computed and compared (Figure 1-5). Before stacking (for both current and reference), the single day stacks with correlation coefficient < 0.6 are taken out.

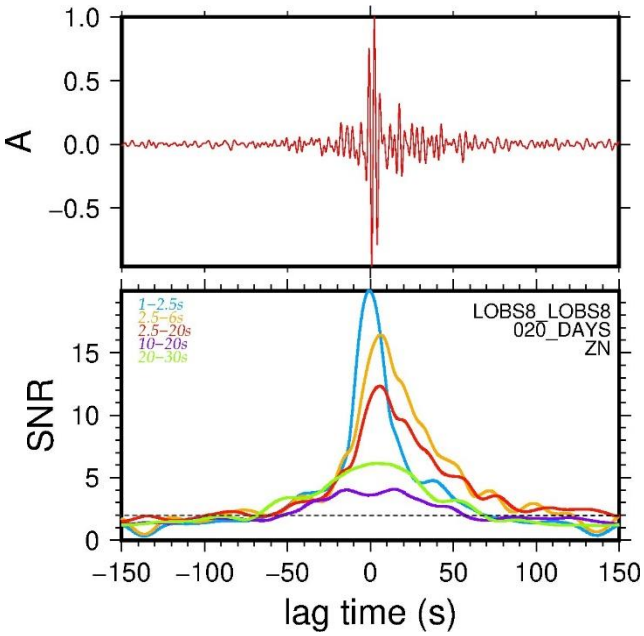

Figure 1-3. Different filters comparison. Waveform of 20 days stack filtering by 2.5-20 s is shown on the top, which has stronger signal on the positive lag. Lag-time dependent SNR is computed on different filtered stacks. 20 days stacks are used.

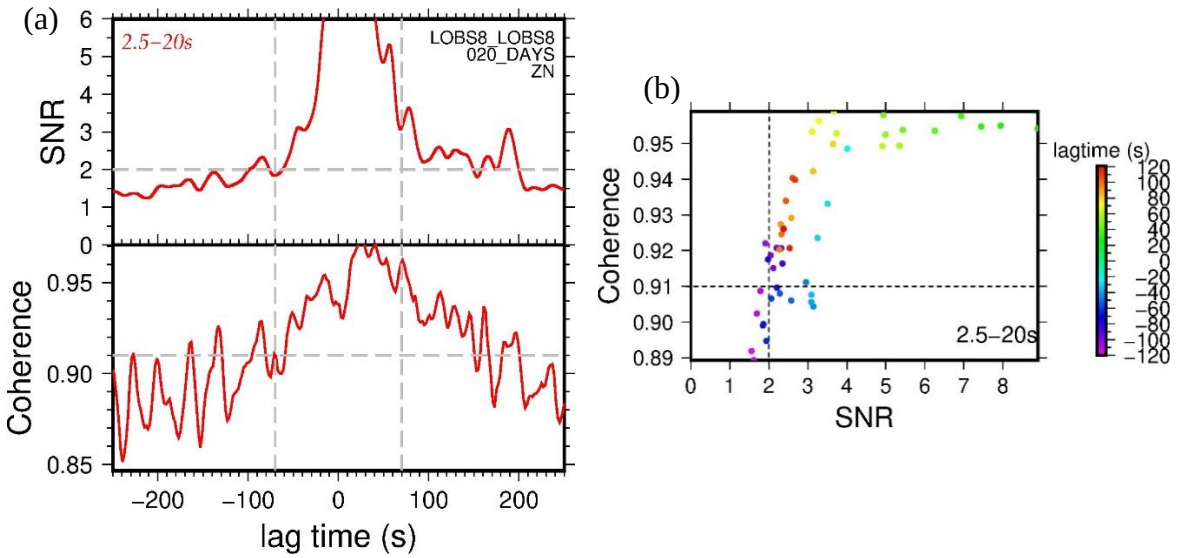

Figure 1-4. Determination of coda wave window and threshold of coherence. (a) Lag-time dependent SNR and coherence. The grey vertical dashed lines at 70 s lag time mark the coda wave window to compute dv/v. Two horizontal dash lines mark the threshold of SNR and coherence. (b) Relationship between SNR and coherence. SNR and coherence between current stack and reference stack at different lag times are computed, denoted by different colors. Threshold of SNR and coherence are marked by the dashed lines.

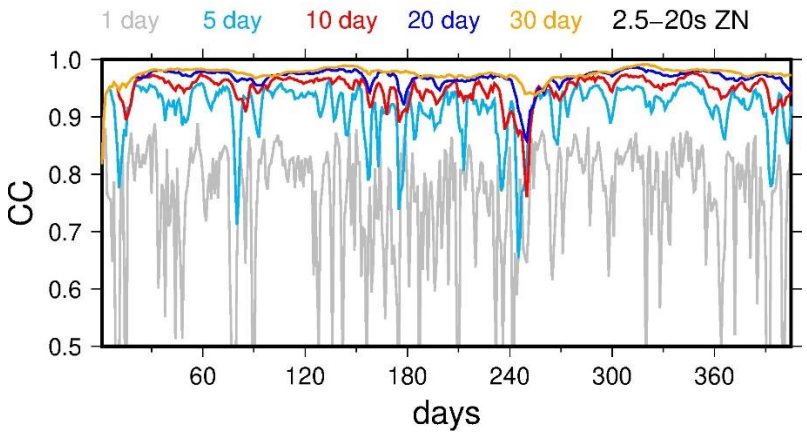

Figure 1-5. Relationship between stack size and correlation coefficient. Correlation coefficients (CC) between different size current stacks (1 day stack, 5 day stack, …, 30 day stack) and reference stack are computed and compared. X-axis shows the deployment days.

During the process, horizontal components of the stations are rotated to be parallel and perpendicular to the coastline. Coda waves are derived from single station vertical-parallel cross correlations, vertical-perpendicular cross-correlations, and parallel-perpendicular cross-correlations. Reference stack is stacked by all the cross-correlations during the deployment. dv/v is computed and averaged. Component averaged dv/v is then averaged from station LOBS3, LOBS7, LOBS8, LOBS9, and all EBSs. LOBS10 is not used because of clock drift, LOBS1 is not used because of data quality, and LOBS6 is not used because its orientation is not able to be determined and therefore its horizontal components cannot be rotated.

1.3 Preliminary result

There are four main SSEs (Warren-Smith et al. 2019) during the deployment, from which SSE2 has bigger slip than the other three SSEs. From the result for 10 days moving window (Figure 1-6), there is a 0.1% velocity decrease at the beginning of SSE2 and a 0.14% velocity increase after that. For each moving window, the value used is at the middle day of the window. Therefore, the velocity variations can have 5 days shift in a 10 days window. The variations suggest a stress decrease caused by a low fluid reservoir before SSE2, and a stress increase after that. During SSE2, fluid releases and result in velocity decrease.

The velocity variations are compared to pressure variations (Figure 1-7) to test if some variations are related to the sea water pressure changes. 7 LOBSs are equipped with absolute pressure gauge. Pressure data recorded by the LOBSs are 2-day lowpass filtered and averaged. Vp/Vs and delay time variations are also compared to the velocity variations to test if they have accordance. The pressure and dv/v variations are different around SSE2 but are similar out of SSE2, implying the variations not related to SSE2 might be caused by sea water pressure changes. The dv/v variations around SSE2 are opposite to the Vp/Vs variations and similar to the delay time variations.

Figure 1-6. Mean and median velocity variations from used stations. From top to bottom 30 days, 20 days and 10 days moving windows of current stacks are used. Four main SSEs during deployment are marked. The biggest event SSE2 is marked by orange.

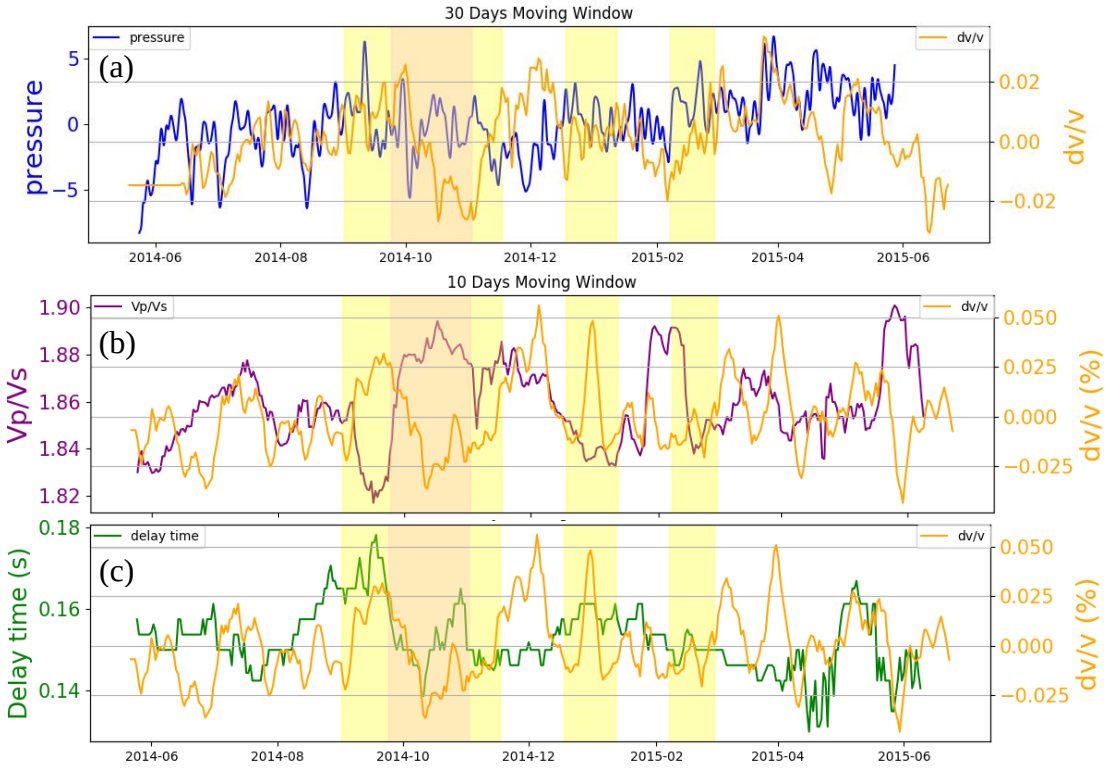

Figure 1-7. Median value of velocity variations compared to other data sets. (a) 30 days moving window dv/v compared to 2-day lowpass filtered pressure. The dv/v values are smoothed by two days window. (b) and (c) 10 days moving window dv/v compared to Vp/Vs and delay time variations (from Zal et al., 2020) respectively. The dv/v values are smoothed by five days window.

Reference

Wallace, L. M., S. C. Webb, Y. Ito, K. Mochizuki, R. Hino, S. Henrys, S. Schwartz, A. Sheehan, 2016. Slow slip near the trench at the Hikurangi subduction zone, Science 352(6286), 701-704.

Coffin, M. F., L. M. Gahagan, and L. A. Lawver, 1998. Present-day plateboundary digital data compilation, Tech. Rep. 174, 5 pp., Univ. of Tex.Inst. for Geophys., Austin.

Williams, C. A., et al., 2013. Revised interface geometry for the Hikurangi subduction zone, New Zealand, Seismol. Res. Lett. 84(6), 1066–1073.

Brenguier, F., M. Campillo, C. Hadziioannou, N. M. Shapiro, R. M. Nadeau, and E. Larose, 2008. Postseismic relaxation along the San Andreas fault at Parkfield from continuous seismological observations, Science 321, no. 5895, 1478-1481.

Lecocq, T., C. Caudron, et F. Brenguier, 2014. MSNoise, a Python Package for Monitoring Seismic Velocity Changes Using Ambient Seismic Noise, Seismological Res. Lett. 85(3), 715-726.

Yates, A. S. (2018). Seismic velocity changes at White Island volcano from ambient noise interferometry (Master's thesis). Victoria University of Wellington.

Clarke, D., Zaccarelli, L., Shapiro, N. M., and Brenguier, F., 2011. Assessment of resolution and accuracy of the Moving Window Cross Spectral technique for monitoring crustal temporal variations using ambient seismic noise. Geophys. J. Int. 186(2):867-882.

Larose, E., Roux, P., & Campillo, M., 2007. Reconstruction of Rayleigh-Lamb dispersion spectrum based on noise obtained from an air-jet forcing. J. acoust. Soc. Am. 122(6)), 3437–3444.

Warren-Smith, E., Fry, B., Wallace, L., Chon, E., Henrys, S.A., Sheehan, A.F., Mochizuki, K., Schwartz, S.Y., Lebedev, S., 2019. Episodic stress and fluid pressure cycling in subducting oceanic crust during slow slip. J. Geophys. Res., Solid Earth.

Levshin and Ritzwoller, 2001. Automated detection, extraction, and measurement of regional surface waves, Pure Appl. Geophys.158(8), 1531–1545.

Zal H., Jacobs K., Savage M.K., Yarce J., Mroczek S., Graham K., Todd E.K., Nakai J., Iwasaki Y., Sheehan A., Mochizuki K., Wallace L., Schwartz S., Webb S., Henrys S., 2020. Temporal and spatial variations in seismic anisotropy and VP/VS ratios in a region of slow slip, Earth Planet. Sci. Lett. 532 115970.

2. Southwestern Okinawa Trough

2.1 Background and data

In east offshore Taiwan, the Philippine Sea Plate subducts beneath the Eurasian Plate along the Ryukyu Trench, forming Ryukyu arc and Okinawa trough by the collision of the subducting slab and Eurasian lithosphere (Figure 2-1 inset). The Philippine Sea Plate is subducting at a rate about 82 mm/yr (Seno, 1993) while the Ryukyu arc retreats southwards because of the oblique subduction. The Okinawa trough is a curved back-arc basin, where the most notable tectonic processes are active extension and rifting within the continental lithosphere. Continental rifting along the Okinawa Trough has occurred in three phases since initiation (Sibuet et al., 1995). The first phase of rifting started in Middle Miocene (12 Ma) or Late Miocene (6 Ma) with the most significant extension of 50 to 75 km. The second and third rifting phases occurred at Late Pliocene-Pleistocene and Late Pleistocene to Recent involving extension of 25 to 30 km in total. Rifting within continental lithosphere is for lithospheric evolution in an extensional stress condition. It can widen the back-arc basin and accumulate more sediment or result in the breaking of continental lithosphere (Kearey et al., 2009).

In this study, we will use the seismic ambient noise data collected at the southwestern edge of the Okinawa Trough where the rifting terminates. From 2010 to 2017, the Institute of Earth Sciences, Taiwan (IES) deployed 34 Ocean Bottom Seismometers (OBS) during different times (Figure 2-1) in Southwestern Okinawa Trough. 29 of them are equipped with differential pressure gauge and 3-component seismometers, and 5 of them are equipped with 3-component seismometers only.

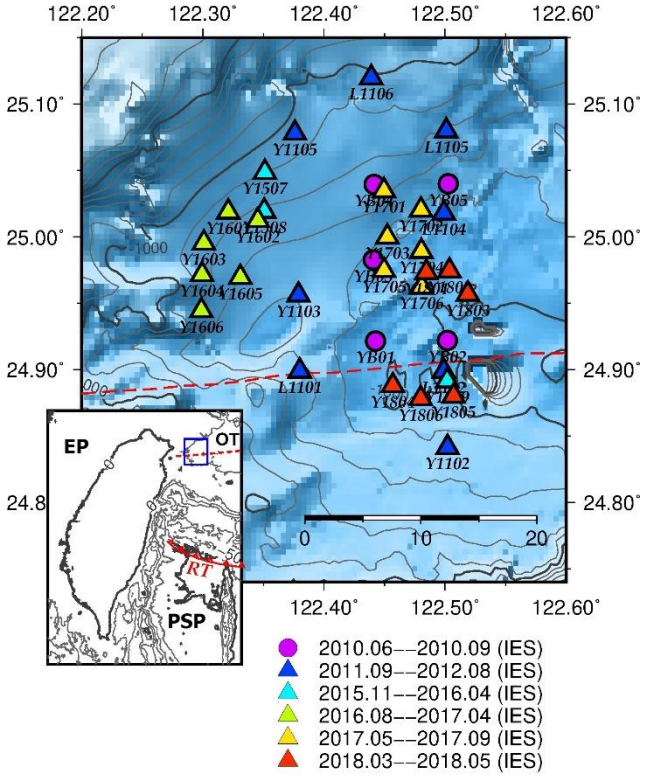

Figure 2-1. Deployment of OBSs in the Southwestern Okinawa Trough. 34 OBSs were deployed during different times denoted by different colors, based on the bathymetry of the seafloor. Circles indicate the instruments equipped with 3-component seismometers only, triangles indicate the instruments equipped with differential pressure gauge and 3-component seismometers. The red dashed line denotes the rifting axis of Okinawa Trough (Sibuet et al., 1998). The deployment region is denoted by the blue rectangle in the inset. EP, Eurasian Plate; PSP, Philippine Sea Plate; OT, Okinawa Trough; RT, Ryukyu Trench.

2.2 Noise cross-correlations

Station pair cross-correlations are computed on both differential pressure gauges and on seismic vertical continuous data. In this study, cross-correlation functions are computed using MSnoise 1.5 (Lecocq et al., 2014). Figure 2-2 shows the cross-correlations derived by pressure gauges and seismic vertical components. The arrivals are considered to be Scholte/Rayleigh waves. The cross-correlation functions derived from seismic vertical components and pressure gauges show similar fundamental mode arrivals, but most of the cross-correlation functions computed using the pressure gauges have higher signal-noise ratios. Therefore, when pressure gauges are available, we use their cross-correlations; otherwise, the cross-correlations derived from the seismic vertical components are used. The earlier arrivals show a velocity close to the sound wave speed in water and they are mostly only observed by pressure sensors. We will prove in Chapter 2.3 that the earlier arrivals couple well with the solid earth instead of just traveling in the sea water by the correction of compliance and tilt noise.

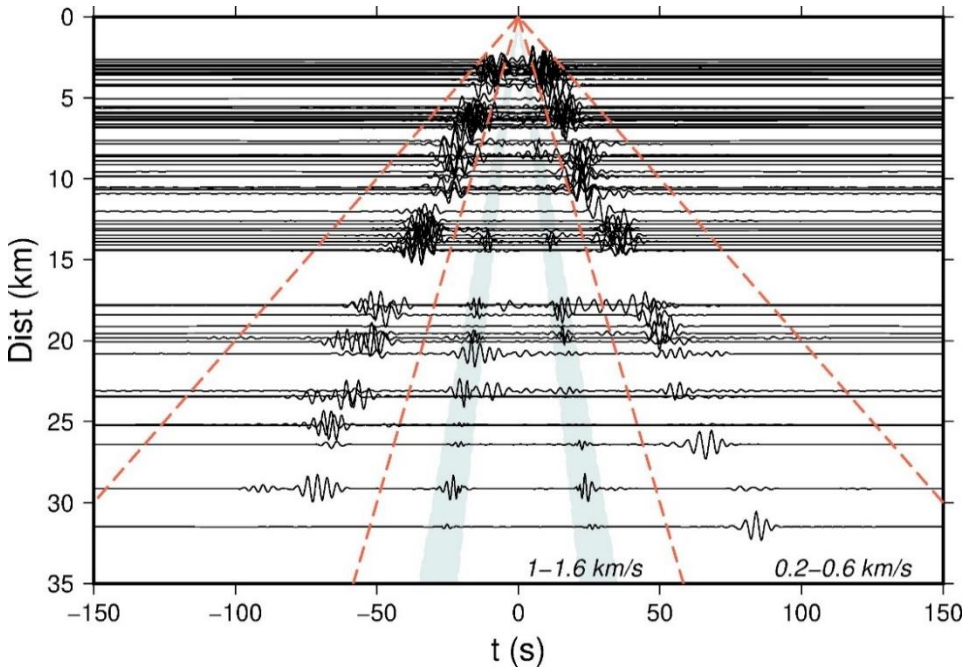

Figure 2-2. Cross-correlation functions computed by the pressure gauges or seismic vertical components of the OBSs plotted as a function of interstation distance, filtered by 1-20 s, showing an earlier arrival with a dominant period of 1-3 s and a velocity of 1-1.6 km/s, denoted by the blue shade, and a later arrival (fundamental mode) with a dominant period of 3-6 s and a velocity of 0.2-0.6 km/s. There are 75 station pair cross-correlation functions.

2.3 Correction of compliance and tilt noise

Compliance noise is from the seafloor deformation caused by the pressure change of the overlying water column. The bottom current moves the sensor to be tilted from the vertical and the current noise recorded by horizontal components project onto the vertical component, which is called tilt noise (Webb., 1998). Crawford et al. (2000) proposed a method to remove the compliance noise by determining the coherence between the pressure and vertical sensors, and subtract the coherent part from vertical sensor. Furthermore, they suggested removing the tilt noise by determining the coherence between the horizontal and vertical sensors, and subtract the coherent part from vertical sensor. These two processes can greatly improve long period signals like earthquakes. Bowden et al. (2016) and Yang et al. (2020) applied this method to retrieve the 1st overtone Rayleigh/Scholte wave from ambient noise data. Fundamental mode Scholte waves couple better with the sea water and therefore they are

suppressed by the compliance removal and the 1st overtone Scholte wave can be retrieved (Bowden et al., 2016). The compliance removal on the vertical component suppresses the waves that have good coupling with sea water.

In this study, the compliance and tilt noise correction is used to test the coupling of the observed waves with the solid earth. If a waves couple well with the solid earth, they can be used to study the underground structure.

The earlier arrivals in Figure 2-2 show a velocity close to the sound wave speed in water. To test if they couple better with the solid earth or the sea water, correction of tilt and compliance noise is conducted on the vertical components of 12 stations pairs from which the latter arrivals (fundamental Scholte waves) are well retrieved but the earlier arrivals are not observed. Compliance noise correction subtracts the coherent signal between pressure and vertical channels from the vertical channel, which can suppress the signal that couples well with sea water. If the faster wave observed by pressure-derived cross-correlations (Figure 2-2) shows up on vertical channel after correction, this wave couples well with the solid earth instead of the sea water because the wave traveling in the sea water should be removed by the compliance noise removal. In the results (Figure 2-3), the cross-correlations derived by compliance corrected data show the early arrivals similar to the ones in Figure 2-2. This suggests that the early arrivals couple well with solid earth and can be used to study the earth structure.

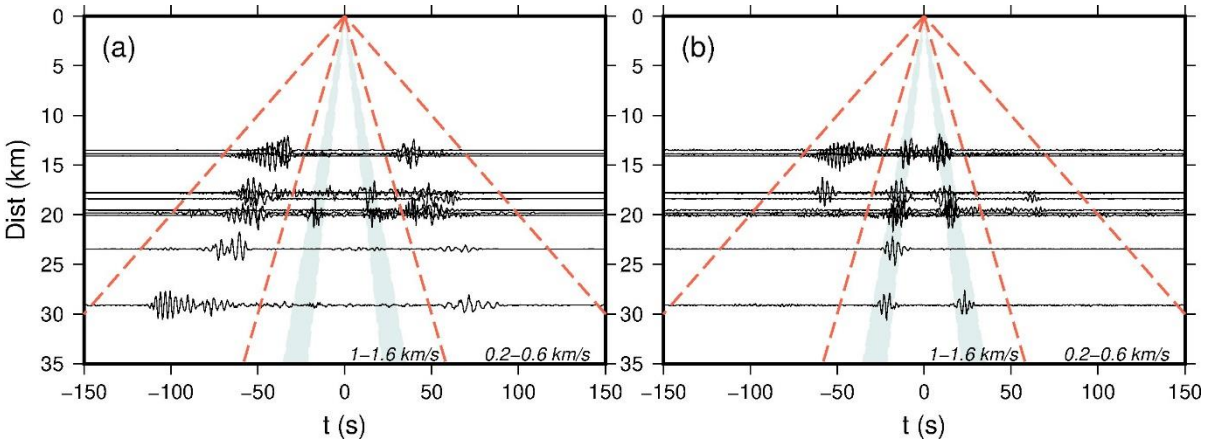

Figure 2-3. Comparison of the cross-correlation functions computed by raw data and compliance corrected data. (a) cross-correlations computed by raw vertical component data. (b) cross-correlations computed by tilt and compliance noise corrected data. After the tilt and compliance noise correction, the later arrivals (fundamental mode Scholte waves) are suppressed and the early arrivals become much clear. This indicates the early arrivals couple well with the solid earth.

2.4 Phase velocity dispersion curves and 1D inversion

The fundamental mode and the 1st overtone Scholte waves are input into Ftan (Levshin and Ritzwoller, 2001), a program designed for processing of seismic surface wave records through methods of spectral and frequency-time analysis, for phase velocity measurement. The longest period is restricted to two times the interstation distance (Bensen et al., 2007; Luo et al., 2015). The samples with low signal to noise ratio (<10) are not used. A forward phase velocity dispersion curve based on a shear wave velocity model (Kuo et al., 2015) and an associated phase velocity dispersion computed by all the cross-correlation functions in the corresponding region are used as references to unwrap the phase. Figure 2-4 shows an example of unwrapping the phase.

The study region is divided into three sub-regions (Figure 2-5) according to the measured phase velocities as well as tectonics: southwest edge of Okinawa Trough, center of the study region and south of the rifting axis. The station-pair path coverages (Figure 2-5) and dispersion curves (Figure 2-6) in

the corresponding sub-regions are displayed by different colors. The averaged dispersion curves (Figure 2-6 (b)) in the three sub-regions are used to invert three 1-D shear wave velocity structures in the corresponding sub-regions.

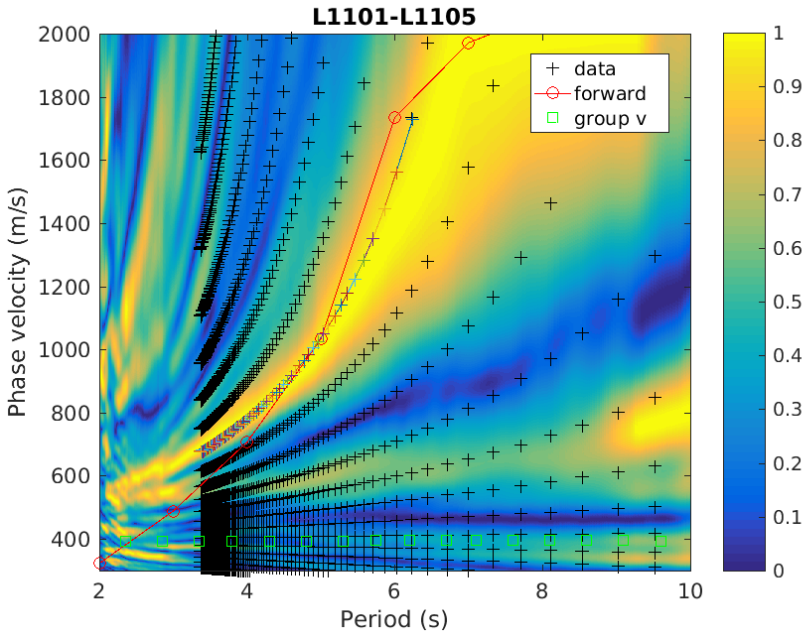

Figure 2-4. Unwrapping the phase of measurement on L1101-L1105. Black crosses display the measured phase velocities with different cycles and the colored crosses are the phase velocities that were chosen. The background colors show associated phase velocity dispersion analysis using all the fundamental mode Scholte waves in the center region, following the method proposed by Park et al., 1998. The red curve with circles showing its samples denotes the phase velocities predicted by a reference model at a site close to our study region (Kuo et al., 2015).

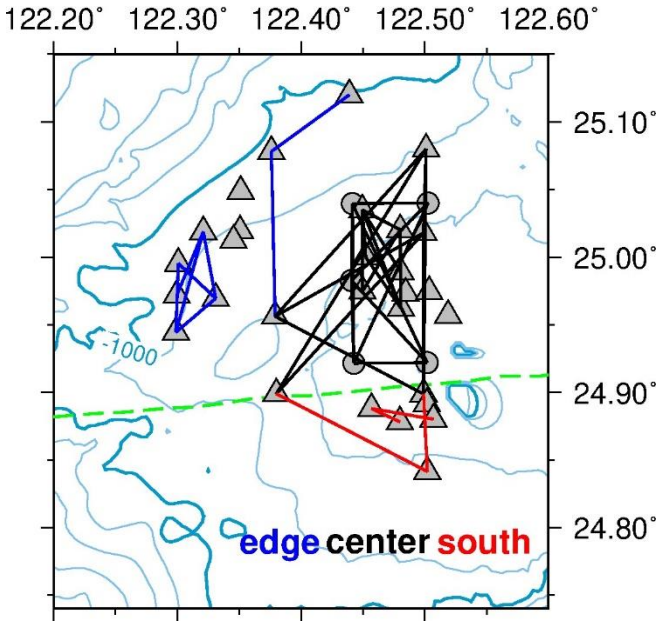

Figure 2-5. Station-pair path coverage in southwest edge of Okinawa Trough (blue), center of the study region (black) and south of the rifting axis (red). The green dashed line indicates the rifting axis.

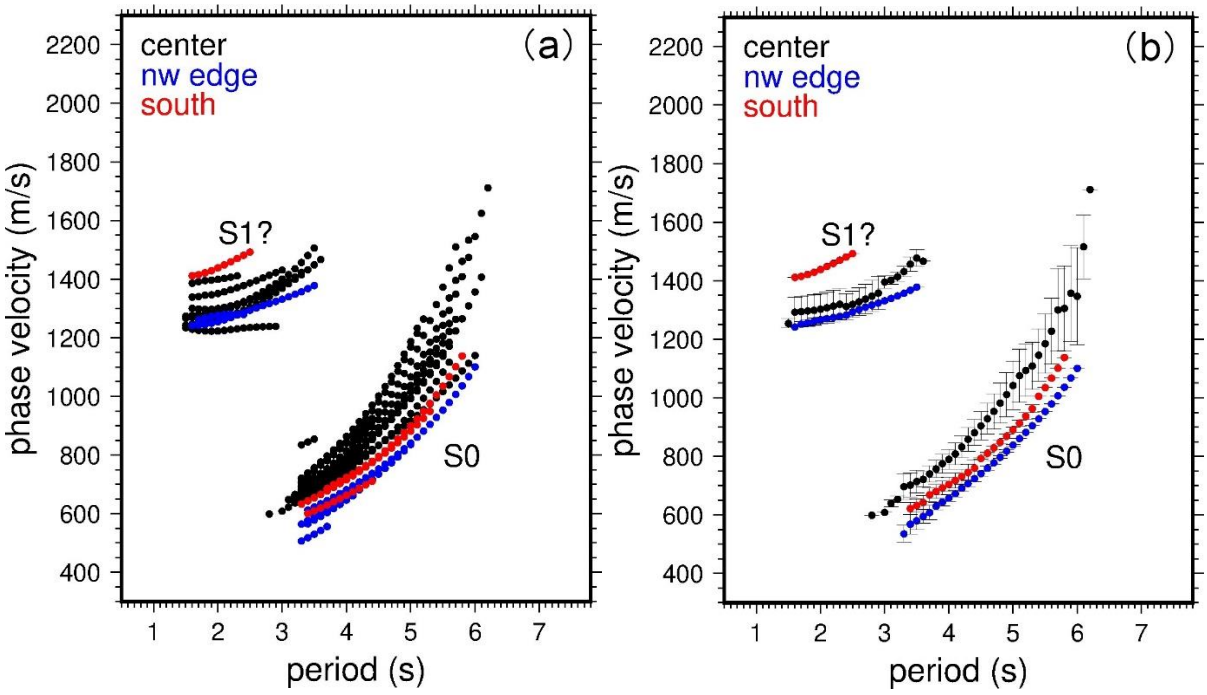

Figure 2-6. Phase velocity dispersion curves measured from the two arrivals in Figure 2-2. (a) dispersion curves measured from the later arrivals -- fundamental mode Scholte waves (S0) and the earlier arrivals – possible 1st overtone Scholte waves (S1); (b) Averaged phase velocity dispersion curves of them, with standard deviation as the errors.

The averaged fundamental mode dispersion curves (Figure 2-6 (b)) are used as the observation for 1D shear wave velocity inversion. The higher mode signals are not used because the data cannot be fitted when they are assumed to be the first overtone and used together with the fundamental mode during the inversion, which suggests they might not be the first overtone of Scholte/Rayleigh wave even though they couple well with the solid earth. The number of data at each period sampling is used as a weighting during the inversion. The Dinver neighbourhood algorithm software code is used for inversion. This 1D inversion software proposes models based on a prior that the user sets and forwards corresponding dispersion curves to test against the data. During the inversion, shear wave velocity and depth of the layers are searched from among wide ranges. The resolution on depth of layers is low because surface waves are not sensitive to interfaces. Further work will set some narrow ranges of depths that will be determined from previous reflection studies.

Figure 2-7 shows the inversion results in the three sub-regions. The shear wave velocity in the center region is slightly higher than that in northwest and south. The velocity difference on the two sides of the rifting axis suggests a stress difference caused by the rifting process or cracking.

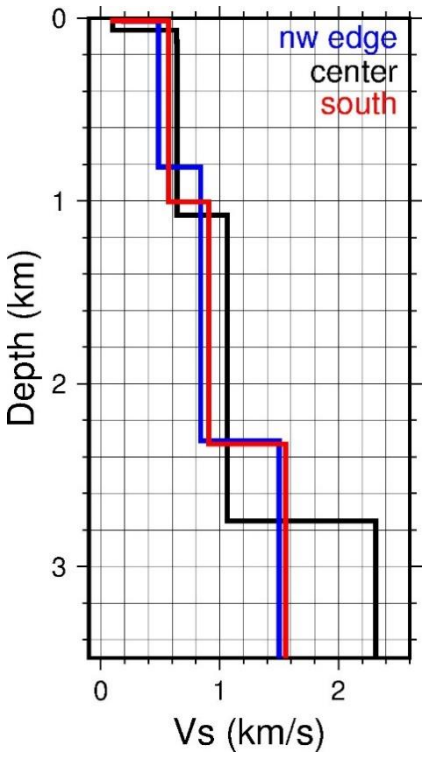

Figure 2-7. Inversion for three average 1D shear wave velocity models in the three sub-regions.

Reference

Bensen, G. D., Ritzwoller, M. H., Barmin, M. P., Levshin, A. L., Lin, F., Moschetti, M. P., Shapiro, N. M. & Yang, Y., 2007. Processing seismic ambient noise data to obtain reliable broad-band surface wave dispersion measurements, Geophys. J. Int. 169, 1239-1260.

Bowden, D. C., M. D. Kohler, V. C. Tsai, and D. S. Weeraratne, 2016. Offshore Southern California lithospheric velocity structure from noise cross-correlation functions, J. Geophys. Res. Solid Earth 121, 3415-3427.

Crawford W. C.,Webb S. C., 2000. Identifying and removing tilt noise from low -frequency (< 0.1 Hz) seafloor vertical seismic data. Bull. seism. Soc. Am. 90(4): 952-963.

Kearey, P., K. A. Klepeis, and F. J. Vine, 2009. Global Tectonics, 3rd ed., Wiley-Blackwell, U. K.

Kuo, B.-Y., W. C. Crawford, S. C. Webb, C.-R. Lin, T.-C. Yu & Chen, L., 2015. Faulting and hydration of the upper crust of the SW Okinawa Trough during continental rifting: Evidence from seafloor compliance inversion, Geophys. Res. Lett. 42, 4809-4815.

Lecocq, T., C. Caudron, et F. Brenguier, 2014. MSNoise, a Python Package for Monitoring Seismic Velocity Changes Using Ambient Seismic Noise, Seismological Res. Lett. 85(3), 715-726.

Levshin, A. L., and Ritzwoller, M. H., 2001. Automated detection, extraction, and measurement of regional surface waves, Pure Appl. Geophys. 158(8), 1531-1545.

Luo, Y., Yang, Y., Xu, Y., Xu, H., Zhao, K., Wang, K., 2015. On the limitations of interstation distances in ambient noise tomography. Geophys. J. Int. 201 (2), 652-661.

Park, C. B., R. D. Miller, and J. Xia, 1998. Imaging dispersion curves of surface waves on multi-channel record: 68th Annual International Meeting, SEG, Expanded Abstracts, 1377-1380.

Seno, T., 1993. A model for the motion of the Philippine Sea plate consistent with NUVEL-1 and geological data, J. Geophys. Res. 98, 17941-17948.

Sibuet, J.C., Hsu, S.K., Shyu, C.T., Liu, C.S., 1995. Structural and kinematic evolution of the Okinawa trough backarc basin. In: Taylor,B. (Ed.), Backarc Basins: Tectonics and Magmatism. Plenum Press, New York, pp. 343-378.

Sibuet, J.-C., B. Deffontaines, S.-K. Hsu, N. Thareau, J.-P. L. Formal, C.-S. Liu, ACT party, 1998. Okinawa Trough backarc basin: Early tectonic and magmatic evolution, J. Geophys. Res. 103, 30,245-30,267.

Webb, S.C., 1998. Broadband seismology and noise under the ocean. Rev. Geophys. 36(1), 105-142.

Yang, X., Luo, Y., Xu, H., & Zhao, K., 2020. Shear wave velocity and radial anisotropy structures beneath the central Pacific from surface wave analysis of OBS records. Earth Planet. Sci. Lett. 534, 116086.